Journal of Solid State Chemistry 182 (2009) 2543–2548

Contents lists available at ScienceDirect

Journal of Solid State Chemistry

journal homepage: www.elsevier.com/locate/jssc

Soft ferromagnet $GdFe_{7.7}Si_{1.3}$ with a $CaCu_5$-to-$Th_2(Ni/Zn)_{17}$ transitional structure

Volodymyr Svitlyk, Yan Yin Janice Cheung, Yurij Mozharivskyj *

Department of Chemistry, McMaster University, 1280 Main Street West, Hamilton, ON, Canada L8S 4M1

ARTICLE INFO

Article history:
Received 14 May 2009
Received in revised form
16 June 2009
Accepted 21 June 2009
Available online 27 June 2009

Keywords:
Gadolinium iron silicide
Structure
Soft ferromagnet

ABSTRACT

$GdFe_{7.7}Si_{1.3}$ was synthesized by arc-melting with subsequent annealing at 1000 °C for 4 weeks. The basic structure of $GdFe_{7.7}Si_{1.3}$ is similar to that of $CaCu_5$ but features random substitution of Gd atoms by Fe_2 dumbbells along the *z*-axis. This random Gd/Fe_2 distribution makes the $GdFe_{7.7}Si_{1.3}$ structure an intermediate between the $CaCu_5$ (no dumbbells) and $Th_2(Ni/Zn)_{17}$ (full ordering of dumbbells) structures. Single crystal X-ray diffraction also points at the formation of a superstructure of a lower symmetry and diffuse scattering between the superstructure spots. $GdFe_{7.7}Si_{1.3}$ orders ferromagnetically at 640 K and exhibits a soft magnetic behavior.

1. Introduction

Magnetocaloric effect (MCE) can be divided into two categories: conventional MCE (CMCE) and giant MCE (GMCE). Magnetic entropy change, ΔS_{mag}, for a CMCE arises from the alignment of magnetic moments and reaches the maximum value around a Curie temperature for a ferromagnetic material [1]. A GMCE can be treated as a CMCE but with an addition of an extra term—structural entropy change, ΔS_{str}, which stems from a first-order structural transition and contributes to the total entropy change, ΔS: $\Delta S = \Delta S_{mag} + \Delta S_{str}$ [1]. GMCE was first observed in the $Gd_5Si_2Ge_2$ phase [2] where a reversible structural transition driven primarily by the formation of Si/Ge–Si/Ge covalent-type bonds is accompanied by a ferromagnetic ordering [3]. Another well-studied GMCE material is an iron-rich $LaFe_{13-x}Si_x$ phase where a magnetic transition is synchronized with a tilting of the Fe-centered [$Fe_{12-x}Si_x$] icosahedra [4].

Phases rich in magnetically active metals are of great interest as a potential magnetocaloric or magnetic materials. "$RE_3(Fe,Si)_{29}$" phases (RE = Y, Sm, Gd, Tb, Dy) are particularly attracting, as they are structurally related to the corresponding $CaCu_5$-type phases, many of which, including $SmCo_5$, possess interesting and useful magnetic properties [5–11]. According to Ivanova and co-coworkers, the "$RE_3(Fe,Si)_{29}$" phases form only after prolong heat treatment at 1000 °C and adopt a monoclinic structure, e.g. "$Tb_3Fe_{24.7}Si_{4.3}$" annealed at 1000 °C for 100 h has $a = 10.55$, $b = 8.45$, $c = 9.63$ Å with $\beta = 96.8°$ [8]. The structural data obtained from the X-ray rocking photographs and/or electron diffraction were inconclusive and provided no atomic parameters. Nevertheless, the "$RE_3(Fe,Si)_{29}$" structures were believed to be derived from the parent $CaCu_5$-type one through the substitution of RE atoms with $(Fe/Si)_2$ dumbbells [5,6,8]. Sm- and Tb-containing phases were reported to order ferromagnetically around 500 K but the corresponding samples were found to be impure, additionally, α-Fe was observed in some alloys [5,6,8]. Interestingly, the $GdFe_7Si_x$ phases with $0 \le x \le 2.5$ (the $Gd_3Fe_{21}Si_x$ composition with $0 \le x \le 7.5$ if normalized to three Gd atoms) were reported to crystallize in a hexagonal $CaCu_5$-type structure with Curie temperatures of around 500 K but they were synthesized by a rapid quenching of the molten alloys on a rotating disk [12]. The $Gd_2Fe_{15}Si_2$ (or $Gd_3Fe_{22.5}Si_3$) phase annealed at 950 °C for 20 days was assigned a hexagonal $CaCu_5$-type structure and had a Curie temperature of 562 K [13].

There seems to be uncertainty not only about the exact structure but also about the exact composition of these and related phases. For example, the V-substituted phases were originally assigned the $RE_2(Fe_{0.91}V_{0.09})_{17}$ composition and a hexagonal superstructure of the $CaCu_5$-type structure, e.g. $a = 24.3$ Å and $c = 20.9$ Å for $Y_2(Fe_{0.91}V_{0.09})_{17}$ [14]. Later studies by the same authors indicated a possible symmetry reduction for the same phases, e.g. $Y_2(Fe_{0.91}V_{0.09})_{17}$ was indexed in an orthorhombic unit cell with $a = 42.09$, $b = 24.30$ and $c = 20.90$ Å [15]. The $Sm_2(Fe_{0.935}Ti_{0.065})_{17}$ phase was reported to be isostructural with the same orthorhombic unit cell [16]. Subsequent electron diffraction studies on $Sm_2(Fe_{0.935}Ti_{0.065})_{17}$ indicated a monoclinic symmetry reduction [17]. The monoclinic symmetry was also assumed for analogous RE–Fe–M phases (RE—rare earth, M—transition metal) whose compositions were now taken as

* Corresponding author. Fax: +1 905 521 2773.
E-mail address: mozhar@mcmaster.ca (Y. Mozharivskyj).

0022-4596/$ - see front matter © 2009 Elsevier Inc. All rights reserved.
doi:10.1016/j.jssc.2009.06.035

$RE_3(Fe,M)_{29}$ [18–21]. Independently studied $Nd_3(Fe_{1-x},M_x)_{29}$ compounds were found to adopt the same monoclinic structure [22–25]. As such, the "$RE_3(Fe,M)_{29}$" phases are similar, both structurally and compositionally, to the "$RE_3(Fe,Si)_{29}$" phases.

Obviously, clarification of structural and compositional features of the "$RE_3(Fe,Si)_{29}$" phases is vital for understanding their physico-chemical properties. Our exploration in this field focused on the synthesis and characterization of gadolinium silicides. Here, we present our results of the single crystal, powder X-ray diffraction and magnetic studies for the $GdFe_{7.7}Si_{1.3}$ phase.

2. Experimental

2.1. Synthesis and X-ray analysis

The starting materials were Gd (99.9 wt%, CERAC Inc.), Fe (99.98 wt%, Alfa Aesar) and Si (99.999 wt%,). Samples with $Gd_3Fe_{27}Si_2$, $GdFe_7Si$, $GdFe_{7.7}Si_{1.3}$, $GdFe_{7.7}Si_{2.3}$ and $GdFe_9$ compositions were arc-melted at least four times in order to achieve homogeneity. Weight losses during arc-melting were less than 0.5%. For heat treatment, the samples were wrapped in Ta foil to prevent reactions with silica tubes.

X-ray powder diffraction was performed on a PANalytical diffractometer with the Co$K\alpha$ radiation in order to eliminate fluorescence associated with the Cu$K\alpha$ radiation. Phase analysis of the annealed at 1000 °C for 4 weeks $Gd_3Fe_{27}Si_2$ sample, which was prepared first, indicated presence of about 10 mass% of α-Fe (W-type structure). In order to establish a composition of the major phase, SEM composition analysis was performed on the single crystals extracted from this sample (Table 1). The SEM results indicated a lower iron concentration in the phase of interest. Subsequently, samples with the $GdFe_7Si$, $GdFe_{7.7}Si_{1.3}$, $GdFe_{7.7}Si_{2.3}$ and $GdFe_9$ compositions were prepared and annealed at 1000 °C for 4 weeks. The phase analysis of the cast and annealed samples is summarized in Table 2.

X-ray diffraction data for single crystals extracted from the $Gd_3Fe_{27}Si_2$, $GdFe_{7.7}Si_{1.3}$ and $GdFe_9$ samples were collected on a STOE IPDS II diffractometer with the Mo$K\alpha$ radiation in the whole reciprocal sphere. Numerical absorption correction was based on the crystal shape obtained from optical face indexing and optimized against equivalent reflections using STOE X-Shape software [26]. Crystal structures were solved and refined using the SHELXS and SHELXL programs [27] respectively (Tables 3–5).

Single crystals from cast $Gd_3Fe_{27}Si_2$, which was prepared first, were indexed in a Th_2Ni_{17}-type cell (Table 2). Crystals extracted from the same sample annealed at 1000 °C for 4 weeks could be indexed in a hexagonal $CaCu_5$-type cell but after taking into account weak superstructure reflections a new, bigger cell could be obtained as discussed below. The same superstructure was found for the crystals extracted from the annealed $GdFe_{7.7}Si_{1.3}$ sample. Refinement of the cell parameters for the basic $GdFe_{7.7}Si_{1.3}$ cell without hexagonal constrains resulted in parameters a and b being equal within 1σ. The hexagonal symmetry was substantiated by the X-ray powder diffraction pattern for annealed $GdFe_{7.7}Si_{1.3}$ (Fig. 1), which showed no peak splitting. Thus, any symmetry reduction into orthorhombic or monoclinic lattices can be excluded for the basic cell of $GdFe_{7.7}Si_{1.3}$.

The basic structure of $GdFe_{7.7}Si_{1.3}$ was successfully solved and refined in a $CaCu_5$-type structure (Tables 3–5, Fig. 2). During the refinement, significant electron density (the 2e site) was observed along the z-axis around the Gd site, additionally, the temperature factor for the Gd site was unreasonably large suggesting a potential deficiency. Assigning Fe atoms to the 2e site and relaxing the occupancy factors for this site and the Gd one improved the refinement. Since the unrestrained fractional occupancies for the two sites added up to 1 within one standard deviation, their total was later constrained to 1 (Table 4). Presence of Si atoms on the Fe 2e site was excluded due to the fact that its occupancy was in good correlation with the Gd occupancy (i.e. the 2e occupancy = 1—the Gd occupancy) and also due to the chemical arguments as discussed below. Si was found to mix statistically with Fe on the 3g site.

During the refinement, large and smeared in the ab plane thermal ellipsoids were observed for the Fe2 atoms on the 2c site at $x=\frac{1}{3}$, $y=\frac{2}{3}$ and $z=0$. Since the atomic vibrations significantly influence intensity of the high-angle reflections, the data were recollected till $2\theta=72.94^\circ$ to obtain more reliable thermal parameters. After the recollection, a significant extra electron density appeared around the Fe2 2c site (7.90 e/Å^3 at 0.51 Å from Fe2), indicating that the Fe2 atoms are more likely to occupy the 6l site (x, 2x, 0) with $x\simeq0.3$ and with the occupancy of $\frac{1}{3}$. The structure refinement with the new Fe2 site significantly improved the residual electron density and lowered the R value ($R_1=0.0388$ vs. 0.0946).

The refined composition for the $GdFe_{7.7}Si_{1.3}$ sample was $Gd_{0.615(5)}Fe_{5.38(6)}Si_{0.39(6)}$ or $Gd_{1.000(8)}Fe_{8.7(1)}Si_{0.6(1)}$ when normalized for 1 Gd atom. The relatively big standard deviations in the composition result from the refinement procedure in which the occupancies of the three sites were refined and the Fe2 site served as an electron density reference. Correlation effects between the site occupancies as well as using the site with the lowest electron

Table 1
SEM compositional analysis of the single crystals from the annealed $Gd_3Fe_{27}Si_2$ sample.

Normalized for:	Single crystal #1[a]	Single crystal #2[a]
1 Gd atom	$Gd_{1.00(2)}Fe_{7.57(5)}Si_{0.81(1)}$	$Gd_{1.00(3)}Fe_{6.77(5)}Si_{1.20(2)}$
3 Gd atoms	$Gd_{3.00(7)}Fe_{22.7(1)}Si_{2.44(4)}$	$Gd_{3.00(8)}Fe_{20.3(2)}Si_{3.60(6)}$

[a] Relatively small standard deviations represent the precision of determining the SEM signal for the corresponding elements but not the accuracy of the compositional analysis.

Table 2
Phase analysis, structure types and cell parameters of the major components for the cast and annealed at 1000 °C samples.

Sample	Treatment	Phases	Structure	Lattice parameters (Å)
$Gd_3Fe_{27}Si_2$	Cast	Gd_2Fe_{17}+Fe	Th_2Ni_{17}	$a=8.468$ (6), $c=8.339$(7)
$Gd_3Fe_{27}Si_2$	Annealed	$GdFe_{7.7}Si_{1.3}$+Fe	"$CaCu_5$"	$a=4.890$ (1), $c=4.164$(1)
$GdFe_{7.7}Si_{1.3}$	Cast	Gd_2Fe_{17}+Si	Th_2Ni_{17}	$a=8.4462$ (7), $c=8.3161$(8)
$GdFe_{7.7}Si_{1.3}$	Annealed	$GdFe_{7.7}Si_{1.3}$	"$CaCu_5$"	$a=4.8931$ (8), $c=4.1659$(8)
$GdFe_9$	Cast	Gd_2Fe_{17}+Fe	Th_2Ni_{17}	$a=8.501$ (1), $c=8.334$(2)
$GdFe_9$	Annealed	Gd_2Fe_{17}+Fe	Th_2Zn_{17}	$a=8.514$ (8), $c=12.487$(11)
$GdFe_7Si$	Annealed	Gd_2Fe_{17}+$GdSi_2$	Th_2Zn_{17}	$a=8.490$ (1), $c=12.409$(2)[a]
$GdFe_{7.7}Si_{2.3}$	Annealed	$GdFe_{7.7}Si_{1.3}$+Fe+X	"$CaCu_5$"	$a=4.8673$ (5), $c=4.1435$(8)[a]

X is an unidentified impurity.

[a] Lattice parameters were obtained from the X-ray powder diffraction data.

Table 3
Crystal data and structure refinement for $GdFe_{7.7}Si_{1.3}$ in the $CaCu_5$-type cell.

Composition loaded	$GdFe_{7.7}Si_{1.3}$ ($Gd_{0.64}Fe_{4.93}Si_{0.83}$)
Composition refined	$Gd_{0.615(5)}Fe_{5.38(6)}Si_{0.39(6)}$
Space group	*P6/mmm*
Lattice parameters (Å)	$a = 4.8931$ (8) $c = 4.1659$ (8)
Volume (Å^3)	86.38 (3)
Crystal size (mm^3)	$0.011 \times 0.018 \times 0.043$
2θ range for data collection	9.62–72.94°
Index ranges	$-8 \le h \le 8$, $-8 \le k \le 8$, $-6 \le l \le 6$
Reflections collected	1517
Independent reflections	114 [$R_{int} = 0.0594$]
Completeness to max 2θ (%)	100.0
Data/restraints/parameters	114/0/14
Goodness-of-fit on F^2	1.317
Final R indices [$I > 2\sigma(I)$]	$R_1 = 0.0388$, $wR_2 = 0.0650$
R indices (all data)	$R_1 = 0.0480$, $wR_2 = 0.0663$
Extinction coefficient	0.027(8)
Largest diff. peak/hole (e/Å^3)	1.873/−2.197

Table 4
Atomic and isotropic temperature (U) parameters for $GdFe_{7.7}Si_{1.3}$ in the $CaCu_5$-type lattice from single crystal diffraction data.

Atom	Site	Occupancy	x/a	y/b	z/c	U (Å^2)
Gd1	1*a*	0.615 (5)	0	0	0	0.0103 (4)
Fe1	2*e*	0.385 (5)	0	0	0.2845(14)	0.0103 (4)
Fe2	6*l*	1/3	0.2926(4)	2*x*	0	0.0112 (8)
Fe3/Si3	3*g*	0.87/0.13(2)	1/2	0	1/2	0.0106 (5)

Table 5
Interatomic distances for Fe1 in $GdFe_{7.7}Si_{1.3}$.

Atoms	Distance (Å)
Fe_1–Fe_1 dumbbell	2.37 (1)
Fe_1–Gd_1	2.981 (6)
Fe_1–Fe_2[a]	2.748 (4)
Fe_1–Fe_3/Si_3	2.606 (2)

[a] The shortest Fe_1–Fe_2 distance is given.

density as a reference did not allow to obtain the true composition. More details on the crystal structure of $GdFe_{7.7}Si_{1.3}$ refined in the basic $CaCu_5$-type cell is available from the Fachinformationszentrum Karlsruhe, 76344 Eggenstein-Leopoldshafen, Germany, (Fax: +49 7247 808 666; e-mail: crysdata@fiz-karlsruhe.de) on quoting the depository CSD number 420655 and from the Supporting Information.

Analysis of the single crystal diffraction data for $GdFe_{7.7}Si_{1.3}$ indicated the presence of both a superstructure and diffuse scattering (Fig. 3). While an automatic indexing of the superstructure reflections yielded a large hexagonal cell with $a = 24.46$ and $c = 20.83$ Å, a honeycomb pattern with extended empty areas in the $(0\,0\,1)_{hex}$ layer (right in Fig. 3) was indicative of a smaller superstructure and twinning. A monoclinic *I*-centered unit cell with $\boldsymbol{a}_{mon} = -\boldsymbol{a}_{hex}-\boldsymbol{b}_{hex}-\boldsymbol{c}_{hex}$, $\boldsymbol{b}_{mon} = \boldsymbol{a}_{hex}-\boldsymbol{b}_{hex}$ and $\boldsymbol{c}_{mon} = \boldsymbol{c}_{hex}$ could be identified, in which a 5-fold superstructure develops along the $\boldsymbol{a}_{mon}$ axis ($\boldsymbol{a}_{super} = 5\boldsymbol{a}_{mon}$). The superstructure reflections of the monoclinic cell had satellite reflections towards the main reflections and a diffuse scattering in-between. The satellite reflections appear to be commensurate with and triple $\boldsymbol{a}_{mon}$. If satellite reflections were treated as regular superstructure reflections, the $\boldsymbol{a}_{mon}$ axis would have to be increased by a factor of 15. The superstructure develops both

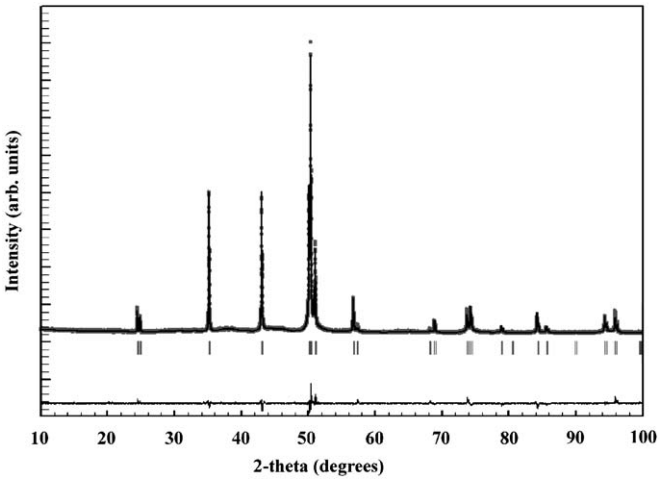

Fig. 1. Experimental powder pattern (dots), Rietveld refinement profile (solid line), Bragg's angle positions (vertical bars) and differential profile (bottom solid line) for $GdFe_{7.7}Si_{1.3}$ in the basic $CaCu_5$-type cell.

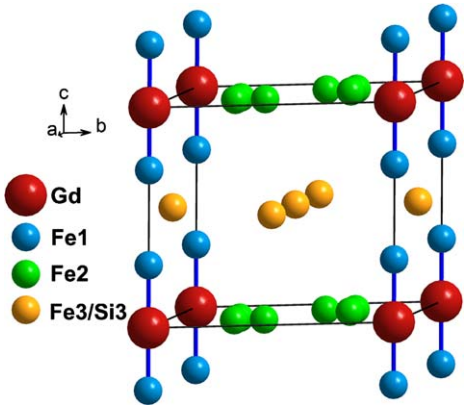

Fig. 2. $GdFe_{7.7}Si_{1.3}$ structure in the basic $CaCu_5$-type cell.

along the $-\boldsymbol{a}_{hex}-\boldsymbol{b}_{hex}-\boldsymbol{c}_{hex}$ and $-\boldsymbol{a}_{hex}-\boldsymbol{b}_{hex}+\boldsymbol{c}_{hex}$ directions for the current choice of the $\boldsymbol{b}_{mon}$ ($= \boldsymbol{a}_{hex}-\boldsymbol{b}_{hex}$) axis and the two twin components are related by 180° rotation around the two-fold axis along $\boldsymbol{b}^*_{hex}$ (left in Fig. 3). Due to the hexagonal symmetry, there are six equivalent choices for $\boldsymbol{b}_{mon}$. Thus, the total number of twin components is 12. Even taking into account twinning, we could not solve and refine the superstructure by the mean of the conventional single crystal X-ray diffraction techniques. Additional complication in solving the superstructure stemmed from the diffuse scattering, which suggests non-correlated positional and/or occupational perturbations between the $CaCu_5$-type unit cells.

The $GdFe_{7.7}Si_{1.3}$ structure in the basic $CaCu_5$-type cell was verified from the powder diffraction data using the FULLPROF software package [28] (Fig. 1 and Supplement Information). Despite the good quality of the diffraction data, the superstructure reflections could not be reliably identified and indexed. However, the diffuse scattering was pronounced and manifested itself as broad bumps around 2θ of 37° and 45°.

2.2. SEM and DTA analysis and magnetic measurements

SEM analysis on the single crystals extracted from the $Gd_3Fe_{27}Si_2$ sample annealed at 1000 °C for 4 weeks was performed

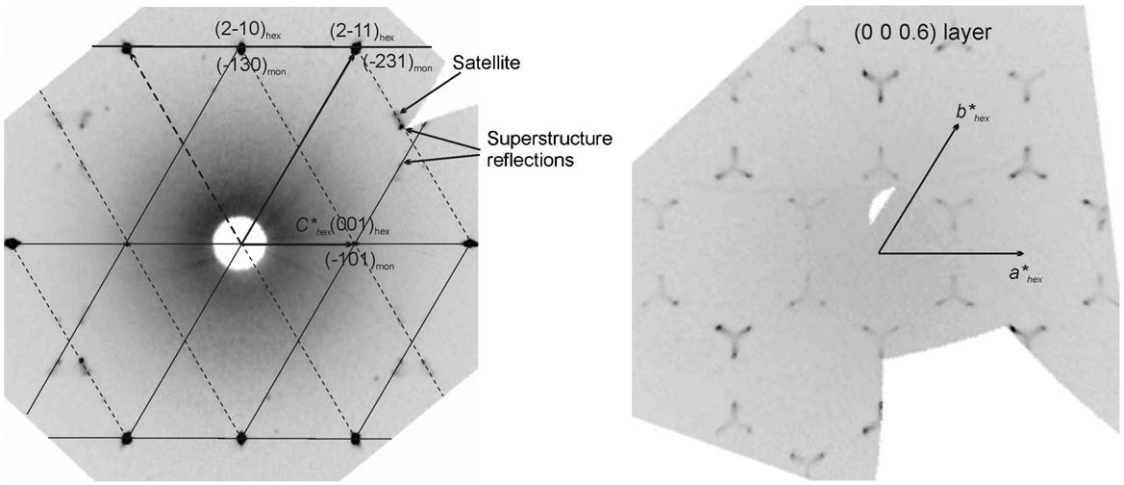

Fig. 3. Reciprocal layers normal to $\boldsymbol{b}^*$ (left) and $\boldsymbol{c}^*$ (right) of the basic hexagonal $GdFe_{7.7}Si_{1.3}$ structure. (Left) Solid inclined lines represent the reciprocal lattice for one twin component, and dashed inclined lines represent the reciprocal lattice for the other twin component. The horizontal lines are the translations that are common for both lattices.

on a Philips 515 microscope and the results are summarized in Table 1.

To establish the formation temperature of $GdFe_{7.7}Si_{1.3}$, differential thermal analysis (DTA) was performed on a Netzsch STA-409 Luxx instrument in high-purity argon gas. The $GdFe_{7.7}Si_{1.3}$ sample was heated from room temperature till 1100 °C at 10 °C/min. No phase transition could be detected (see Supplement Information).

Magnetization in a field-cooled (FC) mode for the polycrystalline $GdFe_{7.7}Si_{1.3}$ sample annealed at 1000 °C for a week was measured on a Quantum Design SQUID magnetometer at 100 Oe field between 700 and 321 K (Fig. 6, on the left). The transition temperature was derived from the $-\delta M/\delta T$ vs. T plot and corresponds to the maximum on the plot. A hysteresis loop for the same sample was measured at 300 K with a field span from −50,000 to 50,000 Oe (Fig. 6, on the right).

3. Results and discussion

3.1. Structure and composition of $GdFe_{7.7}Si_{1.3}$

The basic structure (subcell, Fig. 2) of $GdFe_{7.7}Si_{1.3}$ can be derived from the $CaCu_5$ structure through a partial and random substitution of Gd atoms by Fe_2 dumbbells along the z-axis (Fig. 4). The interatomic distance between the iron atoms of a dumbbell is 2.38(3) Å which is close to $d_{Fe-Fe} = 2.420(1)$ Å in Gd_2Fe_{17} (Th_2Ni_{17}-type) [29]. The separation between Fe atoms of the dumbbells and the neighboring Gd and Fe atoms is also reasonable (Table 5). One can question whether the Gd/Fe_2 substitution has to involve two Fe atoms or can be done with one Fe atom. If only one Fe1 atom is present, then some of the distances to the neighboring atoms along the z-axis become extremely big: 5.354 Å to Gd or 4.163 Å to Fe1 if neighboring Gd is replaced by Fe_2 (or one Fe atom). Obviously, such structural arrangement is unreasonable. The Gd/Fe_2 substitution in $GdFe_{7.7}Si_{1.3}$ is analogous to that reported for $TbCu_7$, where some of the Tb atoms are randomly replaced by Cu_2 pairs [30]. While the composition of the two phases is somewhat different, similar atomic arrangement makes $GdFe_{7.7}Si_{1.3}$ isostructural to $TbCu_7$. The Gd/Fe_2 substitution is also comparable to those found in the Th_2Ni_{17} and Th_2Zn_{17} structures [31,32]. Both in Th_2Ni_{17} and Th_2Zn_{17}, $\frac{1}{3}$ of the Th atoms in the hypothetical $CaCu_5$-type structures is replaced by Ni_2 and Zn_2 dumbbells, respectively (Fig. 4). But in contrast to $GdFe_{7.7}Si_{1.3}$, the substitution is coherent and results in the formation of fully ordered superstructures. The disordered nature of $GdFe_{7.7}Si_{1.3}$ allows to view its structure as a transitional one between the $CaCu_5$ structure, on one hand, and the Th_2Ni_{17} and Th_2Zn_{17} structures, on the other hand. The similarity between these three structures supports (i) the argument that the Gd atoms in $GdFe_{7.7}Si_{1.3}$ are indeed replaced by Fe_2 dumbbells and not by individual Fe atoms and (ii) the fact that Si is absent at the Fe1 site as derived from the single crystal refinement.

The Gd/Fe_2 substitution perturbs the Fe2 site in a way that the Fe2 atoms no longer sit at $x = \frac{1}{3}$ and $y = \frac{2}{3}$ (Fig. 5). Both Gd and Fe2 atoms are located in the same (0 0 1) plane, and if the Fe2 atoms were to remain at $x = \frac{1}{3}$ and $y = \frac{2}{3}$, then its distances to the Gd atoms would be too short while to the Fe2 dumbbells (Fe1 site) would be too long (Fig. 5 left). The Fe2 shifts ($2c \rightarrow 6l$ with $x = 0.285$, Fig. 5 right) allow to make those distances more comparable to the sum of metallic radii ($r_{Fe} = 1.24$ Å [29] and $r_{Gd} = 1.78$ Å [33]). In fact, it can be speculated that the short Gd–Fe2 distances (with Fe2 at $x = \frac{1}{3}$ and $y = \frac{2}{3}$) may be one of the reasons that $GdFe_5$ does not exist. Replacing at least $\frac{1}{3}$ of the Gd atoms with Fe2 dumbbells allows to optimize the distances and stabilize the structure.

The cast $GdFe_{7.7}Si_{1.3}$ sample did not contain the phase of interest. The disordered $GdFe_{7.7}Si_{1.3}$ phase could be obtained after annealing at 1000 °C. This suggests that $GdFe_{7.7}Si_{1.3}$ does not melt congruently and, secondly, that a configurational entropy derived from the Gd/Fe_2 and/or Fe/Si statistical mixtures is likely to be essential in stabilizing the structure. The configurational entropy may also limit the phase existence to high temperatures. Since $GdFe_9$ could not be prepared, Si appears to play a crucial role, but it is difficult to establish whether the electronic or entropical effects associated with the Si presence are more vital for the structural integrity. While statistical mixtures seems to be important, there is also a tendency towards partial ordering as manifested by the existence of the superstructure reflections. But it is not clear whether the Gd/Fe_2, Fe2 and/or Fe/Si3 ordering contribute to the superstructure formation. Weak intensities of the superstructure reflections indicate that the degree of ordering is relatively low, in addition the diffuse nature of the superstructure reflections suggests that the correlation length for this ordering is rather small.

According to the powder diffraction, the basic $CaCu_5$-type lattice of $GdFe_{7.7}Si_{1.3}$ is hexagonal. The monoclinic symmetry

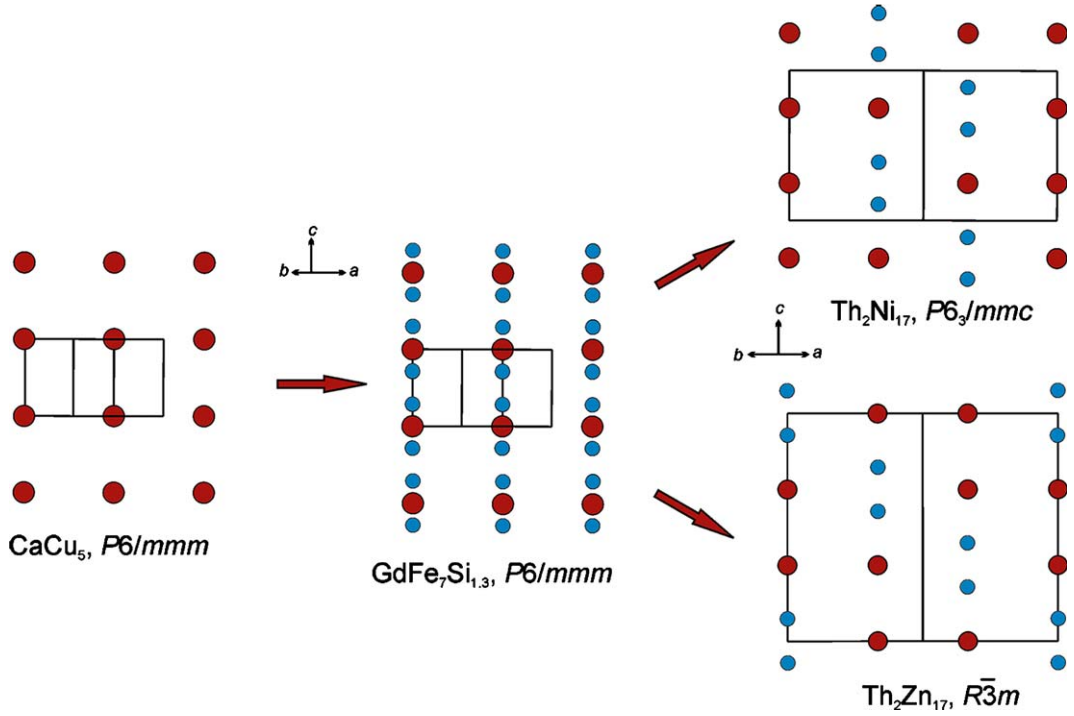

Fig. 4. (black and white version). Relationship between the $CaCu_5$, $GdFe_{7.7}Si_{1.3}$ (basic cell), Th_2Ni_{17} and Th_2Zn_{17} structures. Open circles represent Ca, Gd and Th atoms, black circles represent Fe, Ni and Zn atoms. Only Ca, Gd and Th atoms in one vertical plane are shown. (color online version). Relationship between the $CaCu_5$, $GdFe_{7.7}Si_{1.3}$ (basic cell), Th_2Ni_{17} and Th_2Zn_{17} structures. Dark-red circles represent Ca, Gd and Th atoms, blue circles represent Fe, Ni and Zn atoms. Only Ca, Gd and Th atoms in one vertical plane are shown. (For interpretation of the references to color in this figure legend, the reader is referred to the web version of this article.)

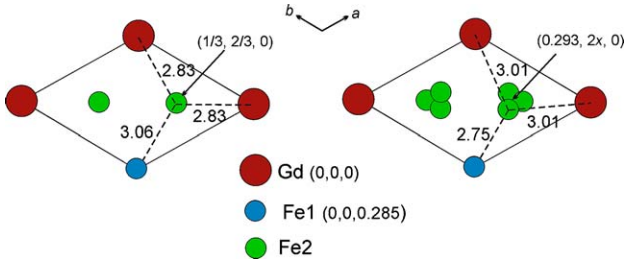

Fig. 5. The (0 0 1) layer and interatomic distances within this layer in $GdFe_{7.7}Si_{1.3}$. (Left) Fe_2 is at $x=\frac{1}{3}$, $y=\frac{2}{3}$, $z=0$ (the original structural model). (Right) Fe2 is at $x=0.293$, $y=2x$, $z=0$ (the final structure model). The occupancy of the Fe2 site is $\frac{1}{3}$ and distances to one Fe_2 atom are shown.

lowering stems from the superstructure formation, which is clearly detectable during the single crystal diffraction. While these observations are consistent with those by Ivanova et al. [5], the monoclinic superstructures appear to be different. The monoclinic superstructure reported by Ivanova et al. [5] is alleged to be identical to that of $Nd_3Fe_{27.7}Ti_{1.5}Mo_y$ [25]. But for $Nd_3Fe_{27.7}Ti_{1.5}Mo_y$, the monoclinic distortion and superstructure formation are different and besides are so pronounced that both features are easily identified from the powder diffraction, which is not the case for $GdFe_{7.7}Si_{1.3}$.

The important issue for the phase discussed here is its composition. Out of the three annealed Si-containing samples, $GdFe_7Si$, $GdFe_{7.7}Si_{1.3}$ and $GdFe_{7.7}Si_{2.3}$, only $GdFe_{7.7}Si_{1.3}$ was found to contain the phase of interest and be pure (Table 2). The annealed $GdFe_7Si$ sample had the Gd_2Fe_{17} phase (Th_2Zn_{17}-type) with a small amount of a secondary phase. The annealed $GdFe_{7.7}Si_{2.3}$ sample, which is Si richer than the $GdFe_{7.7}Si_{1.3}$ one, contained the desired phase with slightly smaller lattice parameters, α-Fe and another unidentified impurity. There seems to exist a small homogeneity region for the phase of interest most likely due to the Fe/Si substitution.

Since the $GdFe_{7.7}Si_{1.3}$ structure is a derivative of the $CaCu_5$-type, its general formula can be written as $Gd_{1-x}Fe_{2x}(Fe_{1-y}Si_y)_5$. Considering that the Gd:(Fe,Si) ratio is 1:9, the solution for x is 0.36 and the Gd occupancy is 0.64, which is within one standard deviation from the X-ray occupancy of 0.61(3). Considering the space requirement for the Fe2 site, it can be speculated that the minimum value of x can be $\frac{1}{3}$. Based on the loading amount of Si, the value for y is 0.1664, which is higher than the refined amount of Si. In summary, the Gd content is well reproduced during the single crystal refinement, however the Si amount is underestimated. While the $Gd_{1-x}Fe_{2x}(Fe_{1-y}Si_y)_5$ formula with $x=0.36$ and $y=0.1664$ highlights the structural relationships and compositional variations well, we have chosen to use the $GdFe_{7.7}Si_{1.3}$ one for its simplicity.

3.1. Magnetic properties of $GdFe_{7.7}Si_{1.3}$

$GdFe_{7.7}Si_{1.3}$ is a ferromagnet with a Curie temperature, T_C, of 640 K (Fig. 6, on the left). A Curie-Weiss fit of the paramagnetic region of this phase cannot be performed reliably due to the limited number of data points in the paramagnetic region. Estimated Weiss temperature falls around 630 K, which is indicative of strong ferromagnetic interactions. A hysteresis loop measured at 300 K (Fig. 6, on the right) shows saturation value of 77.66 emu/g (8.7 μ_B per f.u.) at 50 kOe and remnant magnetization of 2.74 emu/g indicating a soft magnetic nature of this phase.

In intermetallic phases, the effective and saturation magnetic moments of Gd closely resemble the values expected for a free Gd^{3+} ion: $\mu_{eff}=7.92$ μ_B and $\mu=7$ μ_B, respectively [34]. The same can be assumed for Gd atoms in $GdFe_{7.7}Si_{1.3}$. Thus, the 7.7 Fe atoms contribute only 1.7 μ_B in total or 0.22 μ_B /Fe atom to the

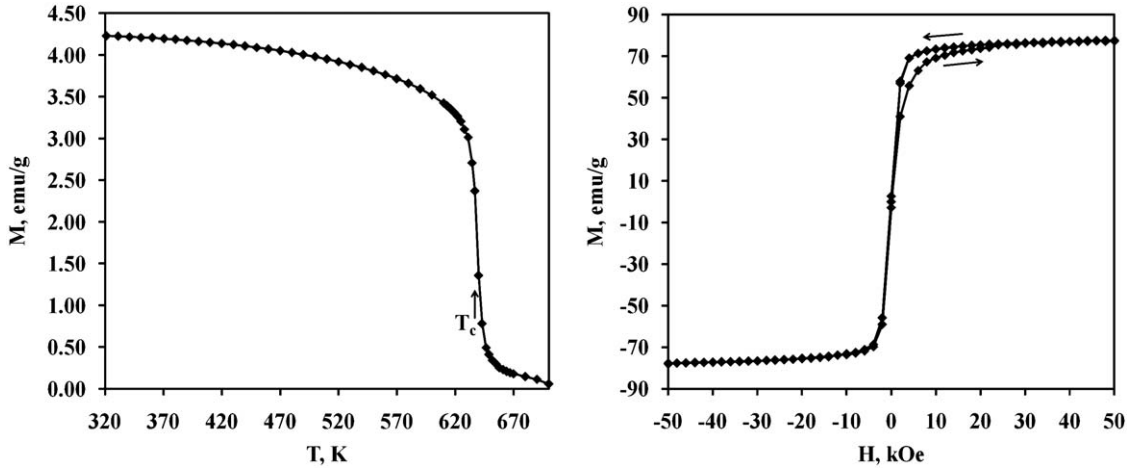

Fig. 6. Magnetization in a field-cooled (FC) mode (on the left) and hysteresis loop at 300 K (on the right) for the polycrystalline $GdFe_{7.7}Si_{1.3}$ sample.

saturation magnetization. Such saturation moments are much smaller than the one observed in pure α-Fe [35] but are comparable to the values found in Fe-containing intermetallic phases (e.g. in $YFe_{8.5}Ti_{1.5}$ [36]). The low saturation moment of Fe atoms in $GdFe_{7.7}Si_{1.3}$ is most likely related to the larger population of the Fe *d*-states as compared to pure iron, but may also be due to a more complex magnetic behavior, e.g. the magnetic moments on the metal sites may not be ferromagnetically coupled.

4. Conclusions

The $GdFe_{7.7}Si_{1.3}$ phase has been synthesized, structurally and magnetically characterized. $GdFe_{7.7}Si_{1.3}$ appears to be a member of the $Gd_{1-x}Fe_{2x}(Fe_{1-y}Si_y)_5$ series with a limited homogeneity range. The basic structure of $GdFe_{7.7}Si_{1.3}$ is of the $TbCu_7$ type. While single crystal experiments point to the formation of a monoclinic superstructure with diffuse scattering, the basic cell remains metrically hexagonal as verified by powder diffraction. The phase exhibits soft magnetic behavior with $T_C = 640$ K. The high Curie temperature renders this material unsuitable for magnetic refrigeration at ambient temperatures.

Acknowledgments

This work was supported by a Discovery Grant from the Natural Sciences and Engineering Research Council of Canada.

Appendix A. Supporting Information

Supplementary data associated with this article can be found in the online version at doi:10.1016/j.jssc.2009.06.035.

References

[1] V.K. Pecharsky, K.A. Gschneidner Jr., A.O. Pecharsky, A.M. Tishin, Phys. Rev. B: Condens. Matter Mater. Phys. 64 (2001) 144406/01–144406/13.
[2] V.K. Pecharsky, K.A. Gschneidner Jr., Phys. Rev. Lett. 78 (1997) 4494–4497.
[3] W. Choe, V.K. Pecharsky, A.O. Pecharsky, K.A. Gschneidner Jr., V.G. Young Jr., G.J. Miller, Phys. Rev. Lett. 84 (2000) 4617–4620.
[4] M.-K. Han, G.J. Miller, Inorg. Chem. 47 (2008) 515–528.
[5] G.V. Ivanova, G.M. Makarova, Y.V. Shcherbakova, Y.V. Belozerov, A.S. Yermolenko, J. Alloys Compd. 260 (1997) 139–142.
[6] G.V. Ivanova, G.M. Makarova, Y.V. Shcherbakova, Y.V. Belozerov, J. Alloys Compd. 309 (2000) 141–146.
[7] G.V. Ivanova, G.M. Makarova, E.V. Shcherbakova, E.V. Belozerov, Fiz. Met. Metalloved. 93 (2002) 71–74.
[8] G.V. Ivanova, G.M. Makarova, Y.V. Shcherbakova, N.N. Shchegoleva, J. Alloys Compd. 360 (2003) 24–29.
[9] G.V. Ivanova, N.N. Shchegoleva, Fiz. Met. Metalloved. 100 (2005) 40–46.
[10] G.V. Ivanova, G.M. Makarova, E.V. Shcherbakova, E.V. Belozerov, Fiz. Met. Metalloved. 99 (2005) 70–74.
[11] K. Strnat, G.I. Hoffer, J.C. Olson, W. Ostertag, J.J. Becker, J. Appl. Phys. 38 (1967) 1001–1002.
[12] J. Yuan, L. Cao, L. Yang, B. Shen, IEEE Trans. Magn. 28 (1992) 2841–2843.
[13] X. Yan, J. Liang, S. Xie, Phys. Status Solidi A 134 (1992) 77–85.
[14] G.V. Ivanova, E.V. Shcherbakova, E.V. Belozerov, A.S. Ermolenko, E.I. Teitel, Fiz. Met. Metalloved. (1990) 67–71.
[15] E.V. Shcherbakova, G.V. Ivanova, A.S. Ermolenko, V. Belozerov, V.S. Gaviko, J. Alloys Compd. 182 (1992) 199–209.
[16] G.V. Ivanova, G.M. Makarova, Y.V. Shcherbakova, Y.V. Belozerov, A.S. Yermolenko, Fiz. Met. Metalloved. 78 (1994) 60–65.
[17] G.V. Ivanova, Y.I. Te'tel, Y.V. Shcherbakova, Phys. Met. Metallogr. 75 (1993) 274.
[18] G.V. Ivanova, G.M. Makarova, Y.V. Shcherbakova, Y.V. Belozerov, J. Alloys Compd. 224 (1995) 29–32.
[19] Y.V. Shcherbakova, G.V. Ivanova, G.M. Makarova, Y.V. Belozerov, A.S. Ermolenko, J. Magn. Magn. Mater. 140–144 (1995) 1099–1100.
[20] G.V. Ivanova, G.M. Makarova, Y.V. Shcherbakova, Y.V. Belozerov, A.S. Yermolenko, J. Alloys Compd. 243 (1996) 95–97.
[21] Y.V. Shcherbakova, G.V. Ivanova, M.I. Bartashevich, V.I. Khrabrov, Y.V. Belozerov, J. Alloys Compd. 240 (1996) 101–106.
[22] C.D. Fuerst, F.E. Pinkerton, J.F. Herbst, J. Magn. Magn. Mater. 129 (1994) L115–L119.
[23] Z. Hu, W.B. Yelon, Solid State Commun. 91 (1994) 223–226.
[24] H.S. Li, J.M. Cadogan, R.L. Davis, A. Margarian, J.B. Dunlop, Solid State Commun. 90 (1994) 487–492.
[25] O. Kalogirou, V. Psycharis, L. Saettas, D. Niarchos, J. Magn. Magn. Mater. 146 (1995) 335–345.
[26] STOE & Cie GmbH, Darmstadt, Germany, 2004.
[27] G.M. Sheldrick, SHELXL97 and SHELXS97, University of Gottingen, Germany, 1997.
[28] J. Rodriguez-Carvajal, IUCr Newsletter 26 (2001) 12–19.
[29] F. Givord, R. Lemaire, J. Less-Common, Metals 21 (1970) 463–468.
[30] K.H.J. Buschow, A.S. Van der Goot, Acta Crystallogr. Sect. B. 27 (1971) 1085–1088.
[31] J.V. Florio, N.C. Baenziger, R.E. Rundle, Acta Crystallogr. 9 (1956) 367–372.
[32] E.S. Makarov, S.I. Vinogradov, Kristallografiya 1 (1956) 634–643.
[33] M. Norman, I.R. Harris, G.V. Raynor, J. Less-Common Metals. 11 (1966) 395–402.
[34] V. Svitlyk, F. Fei, Y. Mozharivskyj, J. Solid State Chem. 181 (2008) 1080–1086.
[35] H. Danan, A. Herr, A.J.P. Meyer, J. Appl. Phys. 39 (1968) 669–670.
[36] R. Revel, E. Tomey, J.L. Soubeyroux, D. Fruchart, T.H. Jacobs, K.H.J. Buschow, J. Alloys Compd. 202 (1993) 57–61.